Journal of Alloys and Compounds 509 (2011) 620–626

Contents lists available at ScienceDirect

Journal of Alloys and Compounds

journal homepage: www.elsevier.com/locate/jallcom

Microstructural evolution of nanostructured $Ti_{0.9}Al_{0.1}N$ prepared by reactive ball-milling

U.K. Bhaskar[a], S. Bid[b], S.K. Pradhan[c,*]

[a] Dept. of Physics, Sreegopal Banerjee College, Bagati, Magra, Hooghly 712148, India
[b] Academy of Technology, G. T. Road, Aedconagar, Hooghly 712121, India
[c] Dept. of Physics, The University of Burdwan, Golapbag, Burdwan 713104, India

ARTICLE INFO

Article history:
Received 24 July 2010
Received in revised form
21 September 2010
Accepted 22 September 2010
Available online 1 October 2010

Keywords:
Mechanical alloying
Rietveld
HRTEM
Nanocrystalline $Ti_{0.9}Al_{0.1}N$
Microstructure

ABSTRACT

Nanocrystalline stoichiometric $Ti_{0.9}Al_{0.1}N$ powder has been prepared by ball-milling the α-Ti (hcp) and aluminum (fcc) powders under N_2 at room temperature. Initially, α-Ti phase partially transformed to the transient cubic β-Ti phase and $Ti_{0.9}Al_{0.1}N$ (fcc) phase is noticed to form after 3 h of milling. Nanocrystalline stoichiometric $Ti_{0.9}Al_{0.1}N$ phase is formed after 7 h of milling. After 1 h of milling, all Al atoms are diffused into the α-Ti matrix. The transient β-Ti phase is noticed to form after 1 h of milling and disappears completely after 7 h of milling. Microstructure characterization of unmilled and ball-milled powders by analyzing XRD patterns employing the Rietveld structure refinement reveals the inclusion of Al and nitrogen atoms into the Ti lattice on the way to formation of $Ti_{0.9}Al_{0.1}N$ phase. Microstructure of ball-milled samples is also characterized by HRTEM. The particle size of $Ti_{0.9}Al_{0.1}N$ phase, as obtained from XRD method, is ~5 nm which is very close to that obtained from HRTEM.

1. Introduction

In recent years, metal nitrides particularly, different (Ti,Al)N compositions have been studied extensively because they exhibit high hardness, good wear resistance and high oxidation resistance at elevated temperatures (over 1075 K) [1–3]. Due to these advantages, (Ti,Al)N has become one of the best coating material for cutting tools, especially for dry and high speed machining [4,5]. To improve the mechanical and tribological properties, various titanium-containing coating materials such as TiN, TiC, TiCN and TiAlN systems are of great interest for a long time due to their high hardness, low friction coefficient and high wear resistance [6–17]. The unique property of TiN makes it an excellent candidate for various applications in the field of hard coating. However, TiN oxidizes easily at higher temperatures which decrease in the wear resistance [18,19] and its performance as hard coating can be improved to a large extent by substituting some Ti atoms by lighter Al atoms having smaller atomic radii [12]. The hardness of (Ti,Al)N coating depends on the Ti/Al ratio. It has been revealed that the hardness increases with increasing Al atoms up to $x = 0.6$ in $Ti_{1-x}Al_xN$ coating. For $x > 0.7$, hardness of the film decreases as the addition of excess Al, favours for phase transition from NaCl structure (TiN) to AlN wurtzite structure [20,21].

It has been reported that (Ti,Al)N coating can be used as the storage node electrode barriers for the fabrication of high-density CMOS memory devices [22–25]. As the alternative material to TiN, (Ti,Al)N can also be applied as the upper electrode for dynamic random access memory (DRAM) devices [26]. Furthermore, (Ti,Al)N coatings exhibit good performance on hydrogen permeation barrier [27] and finds application also in temperature controlling for the satellite [28,29]. So far, TiN based multi-component hard coatings, such as nanocomposite, Ti–Si–N and Ti–Al–N systems have been extensively studied [30] based on their preparation methods and characterizations. However, there is no report on synthesis of nanocrystalline (Ti,Al)N powder by high-energy ball milling the elemental Ti and Al powders in presence of N_2 gas and their nanostructure characterization.

High-energy ball milling has now become one of the conventional methods for production of nanocrystalline materials. Formation of nanocrystalline particles followed by several polymorphic phase transformations in ball-milling process is reasoned by the formation of huge amount of lattice imperfections. X-ray characterization technique based on structure and microstructure refinement is usually preferred [31–37] to measure these lattice imperfections and their nature in order to find the reason for phase transformations in ball-milled nanocrystalline materials. As physical properties of a material depend upon its microstructure, materials with desirable properties can be designed by controlling the microstructure accordingly. In the present study, X-ray diffraction patterns of almost all ball-milled powders, milled for

* Corresponding author. Tel.: +91 342 2657800; fax: +91 342 2657800.
E-mail address: skp_bu@yahoo.com (S.K. Pradhan).

0925-8388/$ – see front matter © 2010 Elsevier B.V. All rights reserved.
doi:10.1016/j.jallcom.2010.09.117

different durations are composed of a large number of overlapping reflections of α-Ti, β-Ti and $Ti_{0.9}Al_{0.1}N$ phases. The Rietveld's analysis based on structure and microstructure refinement [38,39] has been adopted in the present analysis for precise determination of several microstructural defect parameters (changes in lattice parameters, atomic positions, particle sizes, r.m.s. lattice strains, etc.) as well as relative phase abundance of individual phases developed in the course of milling. Microstructure of 12 h ball-milled $Ti0_{.9}Al_{0.1}N$ powder has also been characterized by high-resolution transmission electron microscope (HRTEM).

2. Experimental

Accurately weighed mixture of 0.9 mol fraction of α-Ti (Alfa Aesar, purity 99.5%) and 0.1 mol fraction of Al (Loba Chemie, purity 99.7%) powders was ball milled under N_2 atmosphere in room temperature in a planetary ball mill (Model P5, M/S Fritsch, GmbH, Germany) using a vial of 80 ml volume and 30 balls, both made of hardened chrome steel. The milling was paused after every 15 min to refill the vial with fresh N_2 to maintain constant pressure inside the vial during milling. Homogenized powder mixture was milled for 1 h, 3 h, 5 h, 7 h and 12 h durations to study the rate of growth of (Ti,Al)N phase as well as microstructural changes evolved in the course of milling. The X-ray powder diffraction patterns of unmilled mixture and all ball-milled powders were recorded in step scan (step size 0.02° 2θ; counting time 5–10 s/step) mode using Ni-filtered Cu Kα radiation from a highly stabilized and automated Philips X-ray generator (PW1830) operated at 40 kV and 20 mA. The generator is coupled with a Philips X-ray powder diffractometer consisting of a PW 3710 mpd controller, PW 1050/37 goniometer, and a proportional counter. Microstructure as well as selected area electron diffraction (SAED) patterns of ball-milled samples were characterized using a HRTEM (FEI, TECNAI G2 20, TWIN) operated at 200 kV, equipped with a GATAN CCD camera. Samples were dispersed in ethanol, sonicated and subsequently a drop of it was put on a copper grid for TEM study. Selected area electron diffraction (SAED) pattern and microstructure characterization of 12 h ball-milled sample was also done by analyzing different HRTEM images.

3. Method of analysis

In the present study, we have adopted the Rietveld's structure and microstructure refinement method [40–46] to characterize the microstructure of unmilled and ball-milled samples. In the Rietveld method, the least-square refinements were carried out until the best fit was obtained between the entire observed powder diffraction pattern taken as a whole and the entire calculated pattern based on the simultaneously refined models for the crystal structure(s), diffraction optics effects, instrumental factors, other specimen characteristics. The Rietveld software MAUD [39] is specially designed to refine simultaneously both the structure and microstructure parameters through the Marquardt least-square method. The background of each pattern was fitted by a polynomial function of degree 5. The peak shape was assumed to be a pseudo-Voigt (pV) [38,39,44–46] type profile because it is well established that the observed peak broadening of the sample profile is mainly due to the presence of small particle size and rms strain inside the particles. The particle size and strain broadening can be approximated better with Cauchy and Gaussian type functions, respectively [38,39,44–46]. Being a linear combination of Cauchyian and Gaussian functions, the pV function is the most reliable peak-shape function for profile fitting.

For the Rietveld refinement, an X-ray powder diffraction pattern, containing all three α-Ti (hcp), β-Ti (bcc) and (Ti,Al)N (fcc) phases, was simulated and refined to fit all unmilled and ball-milled experimental patterns. The abundances of different phases were also obtained from the analysis. Refinement of structure and microstructure parameters of simulated pattern continues till convergence is reached with the value of the quality factor, GoF very

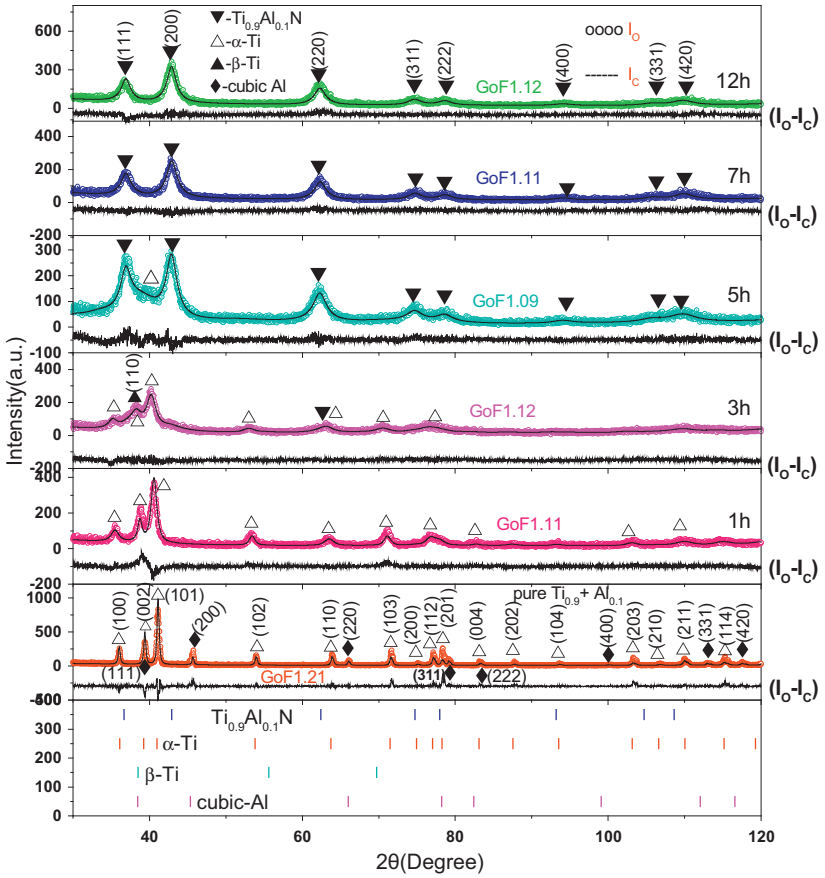

Fig. 1. Rietveld analysis of XRD patterns (—) of unmilled α-Ti and Al mixture ball-milled for different durations. Peak positions of α-Ti, β-Ti, Al and $Ti_{0.9}Al_{0.1}$ N phases are shown at the bottom with small markers (|). Complete formation of $Ti_{0.9}Al_{0.1}N$ is observed after 7 h of milling.

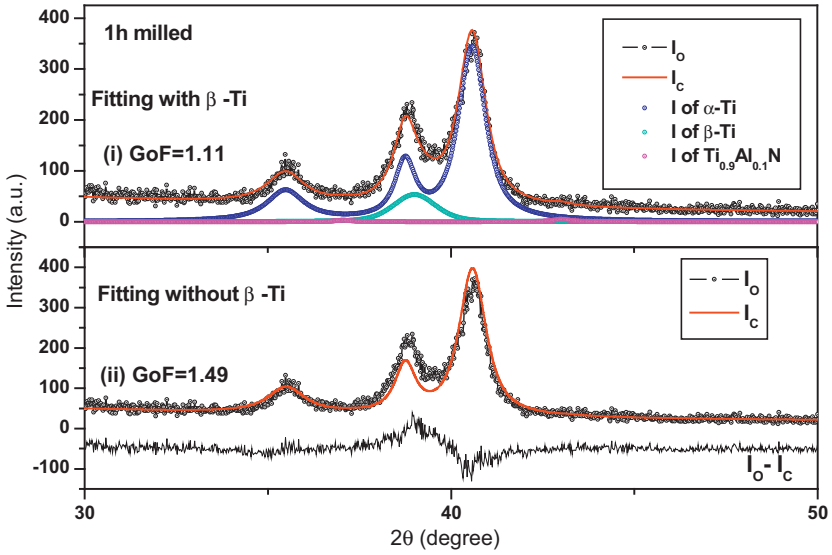

Fig. 2. Upper part: the Rietveld analysis output showing individual contributions α-Ti, β-Ti and $Ti_{0.9}Al_{0.1}N$ phases to the total XRD pattern of 1 h ball-milled sample. Lower part: the Rietveld analysis output showing the fitting quality becomes poor excluding β-Ti phase.

close to unity (in present study, varies between 1.05 and 1.2) which confirms the goodness of fitting.

4. Results and discussion

4.1. Nanostructure characterization by XRD

The XRD powder patterns of unmilled and all ball-milled powders are shown in Fig. 1. The powder pattern of unmilled sample contains only reflections of α-Ti (hcp; ICSD CC 99778) and Al (fcc; ICSD CC 43423) phases and intensities of reflections of respective phases are in accordance with their respective compositions. It is very interesting to note that all Al reflections disappear completely after 1 h of milling and the peak broadening of α-Ti reflections increases continuously with increasing milling time. It clearly indicates that all Al atoms are diffused into α-Ti lattice and a α-Ti based 0.9Ti–0.1Al substitutional solid solution is formed after 1 h of milling. The observed peak broadening of Ti–Al solid solution in the course of milling may be attributed to the effect of both small particle size and lattice strain developed inside the lattice due to constant fracture and re-welding mechanism of mechanical alloying (MA) and substitution of Ti atoms (atomic radius = 0.86 Å) by smaller Al atoms (atomic radius = 0.53 Å). It seems that the nanocrystalline binary Ti–Al solid solution (up to 10 mol%) may be prepared easily at room temperature within 1 h of milling without any contamination either from elemental powders or from milling media. After 3 h of milling, formation of cubic $(Ti_{0.9}Al0.1)N$, similar to cubic TiN phase (ICSD CC 152807) phase is noticed as a minor phase and the peak broadening of major Ti–Al solid solution increases significantly. It ensures that the particle size of Ti–Al solid solution decreases significantly and the probability of nitrogen diffusion into the solid solution matrix increases to a great extent due to increase of surface area of these particles. After 5 h of milling, the $(Ti_{0.9}Al_{0.1})N$ phase appears clearly as the major phase with all its reflections with significant peak broadening. After 7 h of milling, $(Ti_{0.9}Al_{0.1})N$ phase is formed completely and it is interesting to note that the peak broadening reduces very slowly with increasing milling time up to 12 h. It indicates the agglomeration of these nanoparticles in the course of prolonged milling duration.

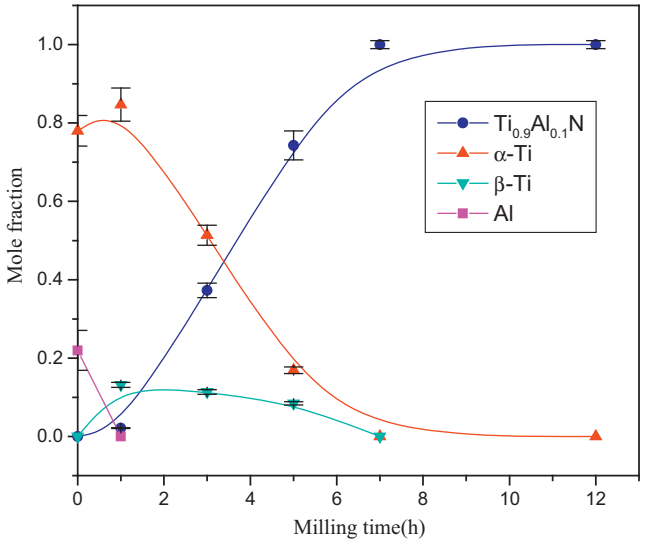

Fig. 3. Variation of phase content (mol fraction) of different phases with increasing milling time towards complete formation of nanocrystalline $Ti_{0.9}Al_{0.1}N$ phase.

The formation of both $(Ti_{0.9}Al_{0.1})N$ phase and transient cubic β-Ti phase is confirmed in 1 h milled sample by the Rietveld refinement analysis as shown in Fig. 2. We have also reported the formation of the transient β-Ti phase in case of preparation of nanocrystalline TiN phase by the same method [31]. Peak positions of both phases are very close to each other and reflections of both phases become broadened significantly after 1 h of milling. As there is no isolated reflection of the nitride and β-Ti phases, it is therefore, very difficult to locate the reflections of nitride phase in this XRD pattern. However, its presence can easily be traced out from the Rietveld analysis as shown in Fig. 2. It confirms that the nitride phase has been initiated within 1 h of milling when all Al atoms diffused into α-Ti-lattice, but the diffusion of N-atom into nitride lattice continues up to 12 h of milling. In the XRD pattern of 3 h milled sample, both (2 0 0) and (3 1 1) reflections of (Ti,Al)N phase appeared clearly but other peaks are either overlapped with α-Ti–Al reflections or broadened significantly.

The relative phase abundances of different phases in unmilled and all ball milled samples with respect to milling time are shown in Fig. 3. According to the Rietveld analysis, contents of α-Ti and Al phases in unmilled sample are 0.79 and 0.21 mol fractions respec-

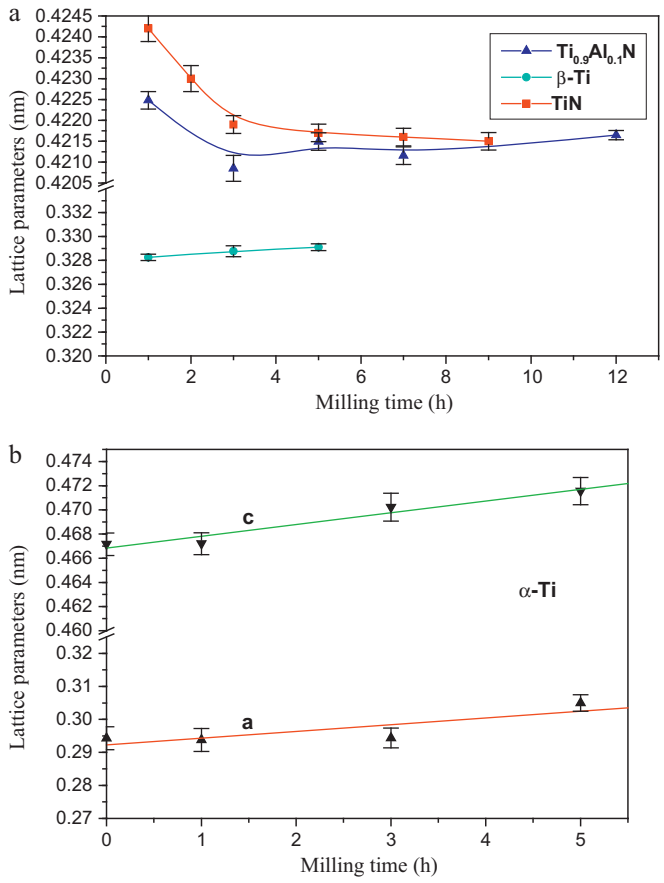

Fig. 4. (a) Variations of lattice parameters of $Ti_{0.9}Al_{0.1}N$, TiN and β-Ti phases with increasing milling time. (b) Variations of lattice parameters of α-Ti phase with increasing milling time.

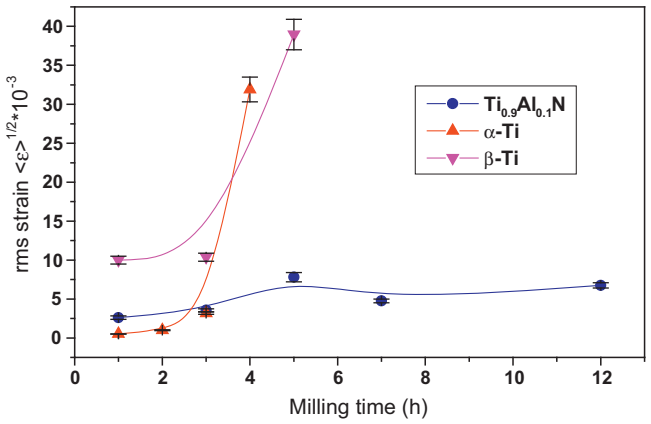

Fig. 6. Variation of rms strain of different phases with increasing milling time.

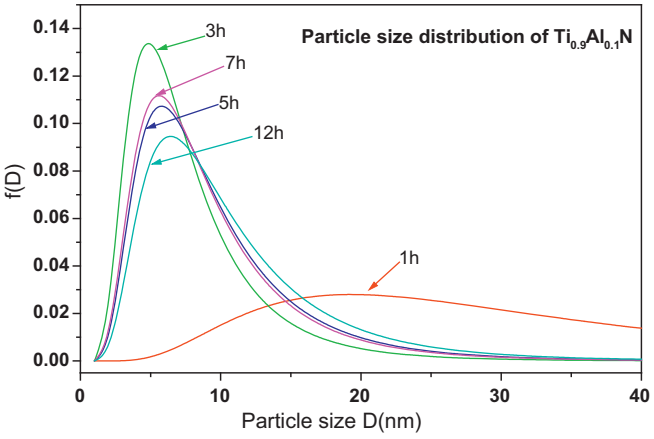

Fig. 7. Distribution of particle size of $Ti_{0.9}Al_{0.1}N$ with milling time.

tively though they were mixed with 0.90 and 0.10 mol fractions. This discrepancy in phase contents arises due to the fact that the aluminum powder covers more surface area than the α-Ti powder during sample mounting. It is evident from the variation that after 1 h of milling, content of Al phase becomes nil and that of α-Ti phase increases to a small extent, which confirms the formation of α-Ti–Al solid solution alloy. Beside this, a significant amount of α-Ti-phase transforms partly to transient cubic β-Ti phase. The formation of nitride phase is initiated after 1 h of milling and then increases very rapidly in the course of milling up to 7 h at the complete expense of α-Ti–Al solid solution phase. Within this period, content of β-Ti phase approaches to nil. This fast rate of growth of nitride phase may be attributed to the adsorption of N_2 atoms on the vast surface area of nanocrystalline α-Ti–Al solid solution particles. The solid solution phase then gradually transforms to the nitride phase in the course of milling and the stoichiometric $Ti_{0.9}Al_{0.1}N$ phase has been formed after 7 h of milling.

The cubic lattice of (Ti,Al)N phase is formed after 1 h of milling with a significantly less value than that of the cubic TiN [31] phase (Fig. 4a). It signifies the diffusion of 0.1 mol fraction of smaller Al atoms into hexagonal α-Ti lattice. After formation, lattice parameter of (Ti,Al)N phase reduces continuously in the course of milling,

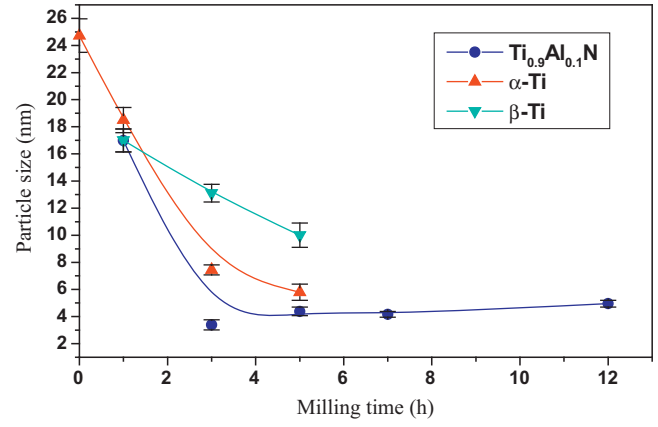

Fig. 5. Variation of particle size of different phases with increasing milling time.

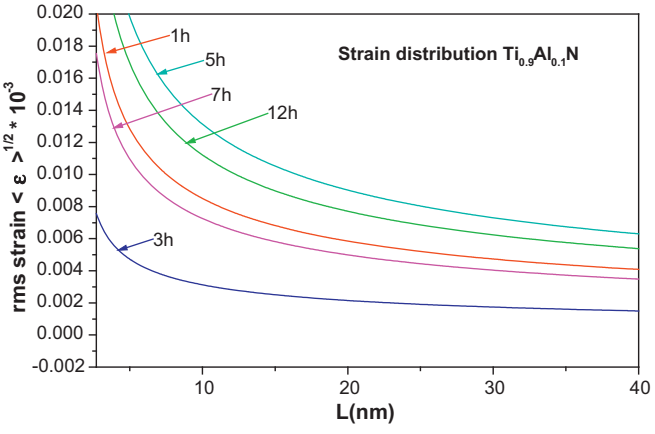

Fig. 8. RMS lattice strain distribution of $Ti_{0.9}Al_{0.1}N$ phase for different milling time.

like the TiN phase. As there is no Al atoms left over for further diffusion into the (Ti,Al)N lattice after 1 h of milling, this contraction in lattice parameter may be caused for one or more of the following reasons: (i) cold-working caused due to high impulsive collision force on (Ti,Al)N lattice during milling, (ii) to achieve a stable atomic configuration, constant re-arrangement of Ti and Al atomic positions inside the lattice due to continuous diffusion of smaller N (ionic radius = 0.13 Å) atoms and (iii) annealing effect on imperfect (Ti,Al)N lattice to make it a perfect lattice by thermal agitation of atoms during milling. It may also be noted that the variation of lattice parameter of (Ti,Al)N phase is almost similar to binary TiN phase but the rate of decrement is different in the lower milling time. However, in the course of milling up to 12 h, lattice parameters of both phases became almost equal, which indicates that the addition of small amount of Al to TiN lattice has a significant influence at lower milling time when there are sufficient nitrogen vacancies. In the long run, when nitrogen vacancy approaches towards nil, influence of Al addition also becomes nil. On the other hand, the continuous linear increment (Fig. 4b) of both lattice constants (c and a) of α-Ti phase obeying the Vegard's law of solid solution reveals the nitrogen diffusion into α-Ti lattice.

The average particle size of α-Ti phase reduces from ~25 nm to ~18 nm within 1 h of milling when the formation of (Ti,Al)N phase is found to be initiated (Fig. 5) with particle size of ~17 nm. After 5 h of milling, particle size of α-Ti phase reduces rapidly to ~6 nm and at the same time that of (Ti,Al)N phase reduces to ~4 nm. It implies that the addition of Al has a great influence on reducing the particle size. In the course of further milling up to 12 h results in slight increase in particle size, owing to agglomeration effect of smaller grains. This is often happen in MA process due to rewelding of highly reactive nanosized grains during collisions. It is also interesting to note that both (Ti,Al)N and β-Ti phases form at the same time and with same particle sizes. So, the possibility of formation of

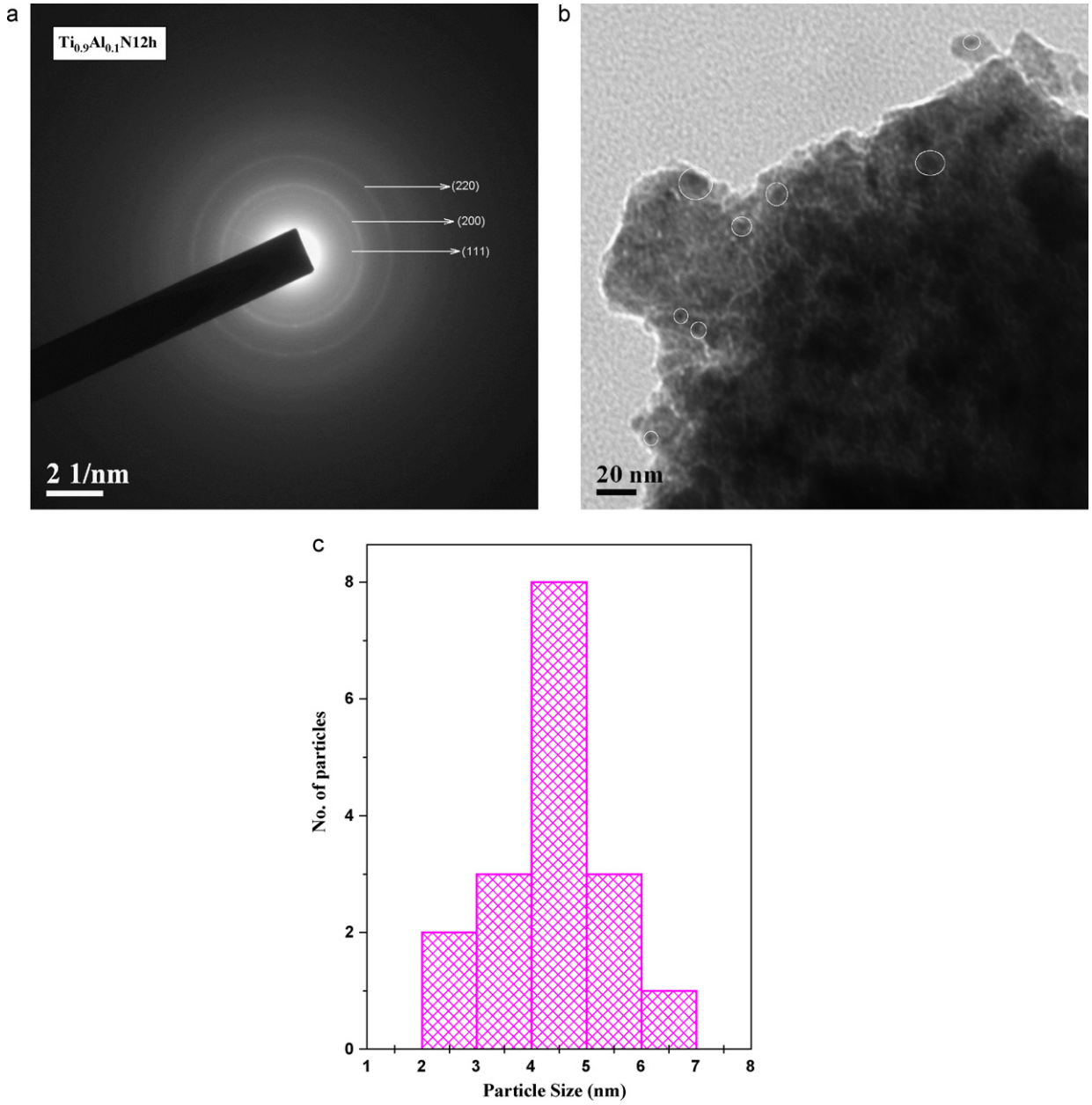

Fig. 9. (a) Selected area electron diffraction (SAED) pattern of nanocrystalline $Ti_{0.9}Al_{0.1}N$ powder after 12 h of milling. (b) TEM image of nanocrystalline $Ti_{0.9}Al_{0.1}N$ powder after 12 h of milling. Spherical particles are marked with white circles. (c) Particle size distribution in 12 h milled (Ti,Al)N sample represented by the histogram.

(Ti,Al)N phase from the transient β-Ti phase may not be ruled out. Particle size of β-Ti phase also reduces very rapidly with increasing milling time. The distribution of particle sizes of (Ti,Al)N phase in different ball-milled samples obtained from the Rietveld analysis are shown in Fig. 6. It reveals from the plot that (Ti,Al)N phase is formed after 1 h of milling with a broad spectrum of particles and in the course of milling, particle size distributions become narrow and after 3 h of milling, almost mono-dispersed particles of average ~5–7 nm size has been obtained. In the progress of milling, a tendency of agglomeration of small particles is noticed and average size of mono-dispersed particles increase slowly with increasing milling time.

Variations of rms lattice strains of different phases with increasing milling time are shown in Fig. 7. The rms strain of (Ti,Al)N phase increases very slowly up to 12 h of milling. It indicates that constant re-arrangement of Ti and Al atoms inside the lattice due to inclusion of N atoms favours to anneal out the lattice strain. However, rms strains in both α-Ti and β-Ti phases increase rapidly with increasing milling time indicating constant diffusion of nitrogen atoms into α-Ti lattice. The β-Ti phase has initiated with a high lattice strain may be due to coherent growth of β-Ti lattice inside the α-Ti lattice with $\langle 1\,1\,1\rangle_{FCC} \| \langle 0\,0\,2\rangle_{HCP}$ shearing mechanism and constant increase in lattice strain in primary α-Ti phase results also in constant growth of lattice strain in secondary β-Ti phase. The distribution of rms lattice strains developed in (Ti,Al)N phase after different durations of ball milling with increasing L ($=na_3$, n is an integer and a_3 is the lattice parameter) are shown in Fig. 8. It can be seen that in all ball milled samples, lattice strain decays very rapidly during progress through lattice. In 3 h milled sample where average particle size is ~5 nm, lattice strain approaches to zero after traveling ~5 nm. It indicates that after traveling this distance, lattice strain annihilates on the particle surface. Due to particle agglomeration afterwards, travel distances (L) of lattice strains in higher time milled samples, also increase considerably.

4.2. Nanostructure characterization by HRTEM

The selected area electron diffraction (SAED) pattern of 12 h milled sample appears properly with relative intensity ratios of cubic (Ti,Al)N reflections only (Fig. 9a). As there is no trace of any other reflections in the SAED pattern, contaminations either from elemental powders or from milling media can be easily ruled out. Like the XRD pattern, intense lines are well resolved though they are sufficiently broadened due to small particle size. However, estimation of particle size and lattice strain from this SAED pattern is not straight forward like the XRD pattern analysis. The average size of spherical particles (marked with white circles) in 12 h milled sample is estimated from the TEM image (Fig. 9b) and the size of

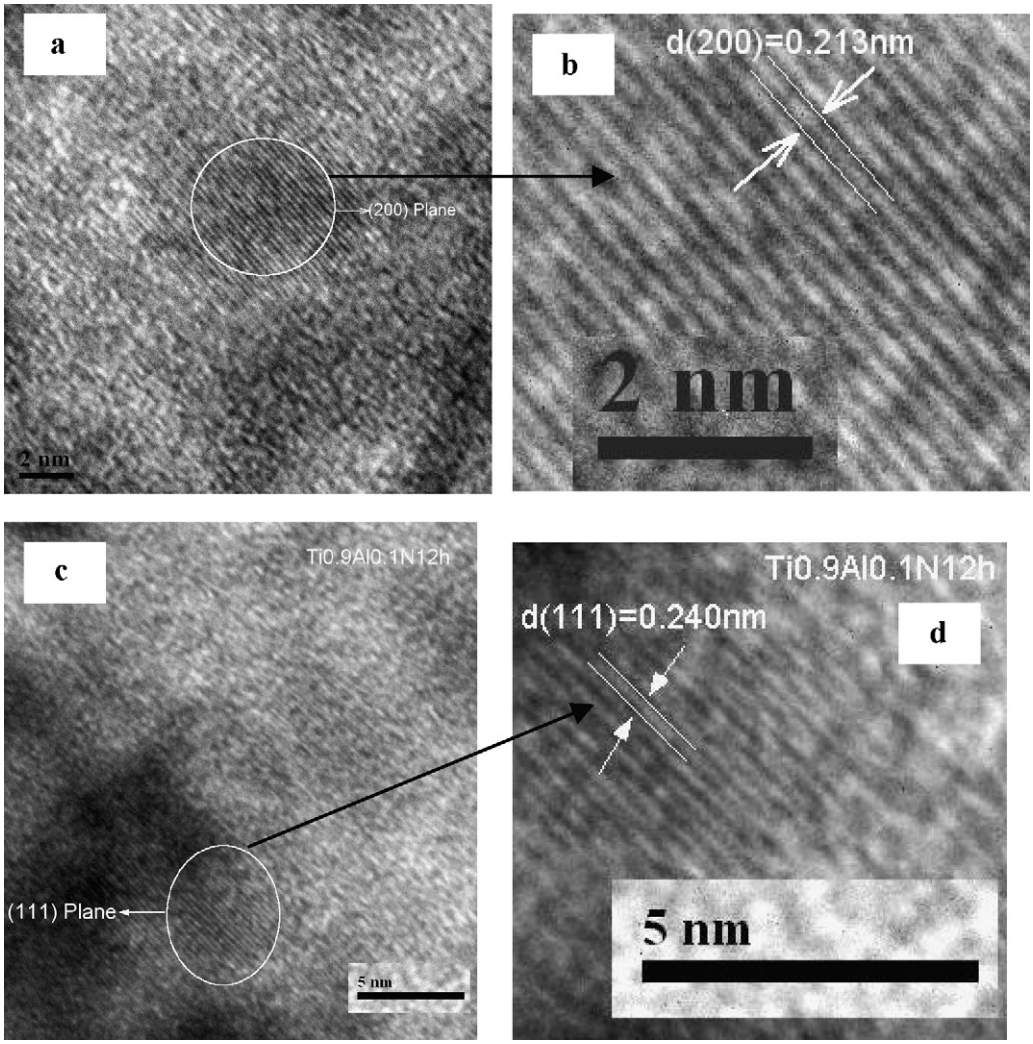

Fig. 10. (a) TEM image shows an isolated $Ti_{0.9}Al_{0.1}N$ particle in 12 h milled sample; (b) HRTEM image confirms it as the (2 0 0) lattice plane; (c) TEM image shows an isolated $Ti_{0.9}Al_{0.1}N$ particle in 12 h milled sample; (d) HRTEM image confirms it as the (1 1 1) lattice plane.

these particles vary between 2 and 7 nm. The distribution of particle size is represented in a histogram (Fig. 9c) where it can be seen that particles are almost mono-dispersed with average size lying between 4 and 5 nm, which is very close to that obtained from X-ray analysis. The HRTEM images (Fig. 10a and b) from a selected area reveals clearly the presence of most intense (2 0 0) plane with *d* value = 0.213 nm. In some other zones (Fig. 10b), presence of lattice imperfections (broken and non-parallel fringes) are also noticed. In some other areas, presence of (1 1 1) plane is also identified with *d* value = 0.240 nm (Fig. 10c and d).

5. Conclusions

Addition of small amount (0.10 mol fraction) of Al to the elemental α-Ti improves overall properties of binary TiN nitride in the nanometer range. This can be achieved easily by high energy ball-milling the α-Ti and Al elemental powders mixture in N_2 atmosphere. The formation of $Ti_{0.9}Al_{0.1}N$ phase is initiated after 1 h of milling through the formation of transient cubic β-Ti phase and complete formation is noticed after 7 h of milling. The nanostructure evolution of all ball-milled samples by the Rietveld analysis reveals that nitride particles are almost mono-dispersed and their average size reduces to 5–7 nm within 3 h of milling. Nanostructure characterization by HRTEM reveals the presence of (Ti,Al)N phase in 12 h milled sample without any contamination. Average size of the spherical particles is found to be ∼4–5 nm which is very close to that obtained from the X-ray analysis.

Acknowledgements

The author SKP wishes to thank to the University Grants Commission (UGC), India for granting DSA-III programme under the thrust area "Condensed Matter Physics including Laser applications" to the Dept. of Physics, The University of Burdwan under the financial assistance of which the work has been carried out. We are also grateful to IIT, KGP for providing the HRTEM facility.

References

[1] F. Mei, N. Shao, L. Wei, G. Li, Mater. Lett. 59 (2005) 2210–2213.
[2] S. Paldey, S.C. Deevi, Mater. Sci. Eng. A 342 (2003) 58–79.
[3] J.M. Castanho, M.T. Vieira, J. Mater. Process. Technol. 143/144 (2003) 352–357.
[4] J.R. Roos, J.P. Celis, E. Vancoille, Thin Solid Films 193/194 (1990) 547–556.
[5] W. Konig, R. Fritsch, D. Kammermeier, Surf. Coat. Technol. 49 (1991) 3164.
[6] M. Nose, T. Nagae, M. Yokota, S. Saji, M. Zhou, M. Nakada, Surf. Coat. Technol. 119 (1999) 296–301.
[7] W. Tillmann, E. Vogli, S. Momeni, Vacuum 84 (2009) 387–392.
[8] J.C. Oliveira, A. Manaia, A. Cavaleiro, Thin Solid Films 516 (2008) 5032–5038.
[9] G.S. Fox-Rabinovich, A.I. Kovalev, et al., Surf. Coat. Technol. 204 (2009) 489–496.
[10] N. Jiang, Y.G. Shen, et al., Mater. Sci. Eng. 135B (2006) 1–9.
[11] J.F. Sun, M.Z. Wang, et al., J. Alloys Compd. 482 (2009) L29–L31.
[12] J. Wang, Z. LiW, H.D. Li, Thin Solid Films 382 (2001) 190–193.
[13] G.G. Fuentes, D. Caĭ ceres, I. Vergara, E. Elizalde, J.M. Sanz, Surf. Coat. Technol. 151 (2002) 365–369.
[14] C.P. Constable, D.P. Lewis, J. Yarwood, W.D. Münz, Surf. Coat. Technol. 184 (2004) 291–296.
[15] L. Karlsson, L. Hultman, J.E. Sundgren, Thin Solid Films 371 (2000) 167–177.
[16] L. Cunha, M. Andritschky, L. Rebouta, R. Silva, Thin Solid Films 317 (1998) 351–355.
[17] F. Quesada, A. Mariño, E. Restrepo, Surf. Coat. Technol. 201 (2006) 2925–2929.
[18] Z. Zhou, et al., Surf. Coat. Technol. 177 (2004) 198–203.
[19] L.A. Donohue, I.J. Smith, W.-D. Münz, I. Petrov, J.E. Greene, Surf. Coat. Technol. 94–95 (1997) 226–231.
[20] A. Kimura, T. Murakami, K. Yamada, T. Suzuki, Thin Solid Films 382 (2001) 101–105.
[21] O. Knotek, M. Bo¨hmer, T. Leyendecker, Mater. Sci. Technol. 105–106 (1988) 481–488.
[22] T.-H. Cha, D.-G. Park, T.-K. Kim, S.-A. Jang, I.-S. Yeo, J.-S. Roh, J.W. Park, Appl. Phys. Lett. 81 (2002) 4192–4194.
[23] D.-Y. Wang, C.-L. Chang, K.-W. Wong, Y.-W. Li, W.-Y. Ho, Surf. Coat. Technol. 120–121 (1999) 388–394.
[24] Q. Yang, D.Y. Seo, L.R. Zhao, X.T. Zeng, Surf. Coat. Technol. 188–189 (2004) 168–173.
[25] D.G. Park, T.-H. Cha, S.-H. Lee, I.-S. Yeo, J.W. Park, S.-D. Kim, J. Vac. Sci. Technol. B 19 (2001) 2289–2294.
[26] Y.J. Lee, S.W. Kang, Appl. Phys. Lett. 86 (2005) 071919–71923.
[27] B.Y. Man, L. Guzman, A. Miotello, M. Adami, Surf. Coat. Technol. 180–181 (2004) 9–14.
[28] R. Karmhag, C.G. Ribbing, Appl. Opt. 38 (1999) 674–678.
[29] M. Brogren, G.L. Harding, R. Karmhag, C.G. Ribbing, G.A. Niklasson, L. Stenmark, Thin Solid Films 370 (2000) 268–277.
[30] J.T. Chena, J. Wanga, C.F. Zhanga, et al., J. Alloys Compd. 472 (2009) 91–96.
[31] U.K. Bhaskar, S. Bid, B. Satpatic, S.K. Pradhan, J. Alloys Compd. 493 (2010) 192–196.
[32] S. Bid, S.K. Pradhan, J. Appl. Cryst. 35 (2002) 517–525.
[33] S. Bid, S.K. Pradhan, J. Appl. Phys. 43 (2004) 5455–5464.
[34] S. Patra, B. Satpati, S.K. Pradhan, J. Appl. Phys. 106 (2009) 034313–34318.
[35] B. Ghosh, S.K. Pradhan, J. Alloys Compd. 486 (2009) 480–485.
[36] B. Ghosh, S.K. Pradhan, J. Alloys Compd. 477 (2009) 127–132.
[37] B. Ghosh, H. Dutta, S.K. Pradhan, J. Alloys Compd. 479 (2009) 193–200.
[38] L. Lutterotti, P. Scardi, P. Maistrelli, J. Appl. Cryst. 25 (1992) 459–462.
[39] L. Lutterotti, MAUD version 2.14, 2009. http://www.ing.unitn.it/∼luttero/maud.
[40] H.M. Rietveld, Acta Cryst. 22 (1967) 151–152.
[41] H.M. Rietveld, J. Appl. Cryst. 2 (1969) 65–71.
[42] H. Toraya, J. Appl. Cryst. 33 (2000) 1324–1328.
[43] B.E. Warren, X-ray Diffraction, Addison-Wesley, Reading, 1969 (Chap. 13).
[44] D.B. Wiles, R.A. Young, J. Appl. Cryst. 14 (1981) 149–151.
[45] R.A. Young, D.B. Wiles, J. Appl. Cryst. 15 (1982) 430–438.
[46] R.A. Young, in: R.A. Young (Ed.), The Rietveld Method, Oxford University Press/IUCr, 1996, pp. 1–38.